Investigation of the Surface and Circulation Impacts of Cloud-Brightening Geoengineering

E. BAUGHMAN

Department of Atmospheric Sciences, University of Washington, Seattle, Washington

A. GNANADESIKAN

Earth and Planetary Sciences, The Johns Hopkins University, Baltimore, Maryland

A. DEGAETANO

Earth and Atmospheric Sciences, Cornell University, Ithaca, New York

A. ADCROFT

Atmospheric and Oceanic Sciences Program, Princeton University, Princeton, New Jersey

(Manuscript received 21 May 2011, in final form 1 March 2012)

ABSTRACT

Projected increases in greenhouse gases have prompted serious discussion on geoengineering the climate system to counteract global climate change. Cloud albedo enhancement has been proposed as a feasible geoengineering approach, but previous research suggests undesirable consequences of globally uniform cloud brightening. The present study uses GFDL's Climate Model version 2G (CM2G) global coupled model to simulate cloud albedo enhancement via increases in cloud condensation nuclei (CCN) to 1000 cm^{-3} targeted at the marine stratus deck of the Pacific Ocean, where persistent low clouds suggest a regional approach to cloud brightening. The impact of this regional geoengineering on global circulation and climate in the presence of a 1% annual increase of CO_2 was investigated. Surface temperatures returned to near preindustrial levels over much of the globe with cloud modifications in place. In the first 40 years and over the 140-yr mean, significant cooling over the equatorial Pacific, continued Arctic warming, large precipitation changes over the western Pacific, and a westward compression and intensification of the Walker circulation were observed in response to cloud brightening. The cloud brightening caused a persistent La Niña condition associated with an increase in hurricane maximum potential intensity and genesis potential index, and decreased vertical wind shear between July and November in the tropical Atlantic, South China Sea, and to the east of Japan. Responses were similar with CCN = 500 cm^{-3}.

1. Introduction

Remedial geoengineering strategies refer to purposeful modifications to the physical climate system designed to offset the effects of anthropogenic radiative gas emissions. One such proposal is modulation of solar radiation that has received considerable attention; these ideas seek to restore top-of-atmosphere radiation balance by increasing shortwave reflectivity. Previous researchers have examined the potential to artificially inject sulfate aerosols into the stratosphere to mimic the reflective cooling caused by volcanic eruptions (Crutzen 2006; Lane 2006; Rasch et al. 2008) but the uncertainty in the climate response coupled with a long atmospheric lifetime are considerable risks (Boyd 2008; Robock 2008).

There has been particularly vigorous discussion of cloud albedo enhancement, also known as cloud brightening, which has been proposed as a method to increase the albedo of persistent low-altitude marine stratocumulus clouds (Latham 1990, Latham 2002). Cloud brightening has received considerable attention primarily

Corresponding author address: E. Baughman, Department of Atmospheric Sciences, University of Washington, 408 ATG Building, Seattle, WA 98195.
E-mail: eowynb@atmos.washington.edu

DOI: 10.1175/JCLI-D-11-00282.1

because it is considered technologically and financially more feasible than other radiative geoengineering approaches, including stratospheric sulfur injections (Bickel and Lane 2009). Based on previous modeling studies, cloud brightening is thought to be reasonably safe and easy to cease (Boyd 2008). However, to date only a few modeling simulations have been conducted (Kravitz et al. 2011), the analyses for which have been restricted to surface responses. Both the American Meteorological Society and the American Geophysical Union have issued policy statements encouraging more sophisticated simulations to increase understanding of the impact of regional near-surface radiative perturbations (AMS 2009). Recent proposals for cloud modification hardware (Salter et al. 2008) and field experiments (Latham et al. 2012) underscore the need for better knowledge of potential consequences.

Previous researchers have employed global climate models to explore the potential meteorological and climatological impacts of cloud albedo enhancement. Early work used uncoupled atmosphere models to examine the ability of cloud brightening to moderate the radiation balance at the top of the atmosphere (Latham et al. 2008). Only two previous studies have used fully coupled global circulation models to investigate the climate response (Jones et al. 2009; Rasch et al. 2009). Jones et al. (2009) considered the response simulated by the Hadley Centre Global Environment Model version 2 (HadGEM2) with cloud condensation nuclei (CCN) increased from around 100 to 375 cm^{-3} in the North Pacific, South Pacific, and South Atlantic, separately and together. Jones et al. (2009) used an A1B forcing trajectory (Houghton et al. 2001) to simulate anthropogenic greenhouse gas emissions. They found that increasing CCN produced a significant decrease in precipitation in South America. Rasch et al. (2009) examined the climate response simulated by the Community Climate System Model, version 3 (CCSM3) with CCN increased from 150 (Collins et al. 2004) to 1000 cm^{-3} in regions similar to Jones with carbon dioxide that increased to double preindustrial concentrations. Their results showed no significant precipitation response in South America, but a strong shift in precipitation patterns in the equatorial Pacific. Jones et al. (2009) and Rasch et al. (2009) both observed a decline in global averaged surface temperature (from noncloud-brightened conditions) of 0.58° and 0.94°C, respectively. The largest cooling occurred in the Arctic (2°–4°C in each study) with a secondary maximum in the enhanced cloud albedo regions (0°–1° and 0°–2°C, respectively). The continents were cooled relative to the noncloud-brightened cases by 0.5°–2.5° (Jones et al. 2009) and 1°–2°C (Rasch et al. 2009). The oceans in each study were subject to a 0°–1°C surface cooling when cloud brightening was in effect.

The present study uses a fully coupled version of the Geophysical Fluid Dynamics Laboratory Climate Model version 2G (GFDL CM2G) global circulation model, which has not been previously used to investigate the climate response to cloud brightening. It expands upon the analyses in previous studies by considering, in addition to surface temperature and precipitation changes, changes in the atmospheric circulation in the equatorial Pacific (the Walker circulation), changes in theoretical maximum potential hurricane intensity in the Atlantic and Pacific basins, and more sophisticated statistical analysis. The present study is undertaken in the spirit of scientific inquiry. It seeks to understand the response of the simulated climate system to a relatively novel, regionalized perturbation occurring in the lower atmosphere. This paper is also among the first to explore how the response differs depending on how the concentration of cloud particles is adjusted. Ultimately the goal is to better understand the global climate system response to a localized radiative forcing in the boundary layer and lower troposphere, and how this response compares to the effects of well-mixed absorbing gases.

2. Theoretical basis

Cloud brightening relies on physical mechanisms concerning aerosol interactions with shallow clouds. Twomey (1974) showed that aerosols introduced to a cloud act as cloud condensation nuclei, which prompt the formation of more numerous but smaller droplets as the total liquid content of the cloud is condensed onto many more nuclei. Condensation nuclei, such as sea salt droplets, which are injected into clean marine stratus clouds, will preferentially act as cloud condensation nuclei (Bower et al. 2006).

As the concentration of cloud condensation nuclei increases, the average effective radius of cloud droplets tends to decrease, particularly in shallow clouds with limited liquid content (Twomey 1977). This results in an increase in shortwave reflectivity (Twomey 1974, Twomey 1977). The addition of cloud condensation nuclei also leads to cloud droplets that are generally smaller and of more uniform size, which tends to suppress coalescence processes within the cloud (Albrecht 1989). Diminished coalescence may suppress precipitation and enhance cloud longevity (Albrecht 1989), which may further increase the time-averaged albedo over the open ocean. All else being equal, an increase in albedo is a direct cooling influence on the climate system (Hartmann 1994).

The actual efficacy of such a scheme is uncertain. Recent work suggests that regional wind patterns will greatly reduce the number of sprayed droplets that

eventually become CCN (Korhonen et al. 2010). However, large eddy simulations (LESs) to resolve cloud processes frequently demonstrate the Twomey and Albrecht effects on stratus cloud shortwave reflectivity (Wood 2012). Observations of smoke interactions with clouds likewise suggest cloud brightening is physically possible (Ghate et al. 2007), although these observations are limited. The well-attested phenomenon of ''ship-tracks'' where enhancements in cloudiness seen in the wake of ships [see recent review by Peters et al. (2011)], also supports the general idea of aerosols enhancing cloudiness in marine boundary layers. It should be noted, however, that the exact mechanism of such enhancement remains subject to debate (Ackerman et al. 2000) and is also unclear whether these effects would scale up from the small spatial scales associated with ship tracks to entire regions.

A major uncertainty in the cloud-brightening mechanism primarily resides in the ability to continuously, effectively deliver condensation nuclei and for those nuclei to become incorporated into marine clouds. Efficacy may also be diminished by cloud dynamical processes which determine how aerosols influence cloud longevity, optical depth, liquid water path, and reflectivity. These processes depend on the aerosol and cloud regime; recent literature indicates there is still considerable uncertainty in aerosol-cloud interactions (e.g., Ackerman et al. 2004; Small et al. 2009; Wood 2007; Stevens and Feingold 2009; Wood 2012). As envisioned, the scale and assumed efficacy of the undertaking represent a probable maximum of cloud modification, or of any similarly ambitious geoengineering scheme. This approach has the advantage of quantifying the limits of beneficial effects while drawing attention to the unintended consequences.

3. Methods

a. Model design

The model used in this study is the fully coupled atmosphere–land–ocean–ice global model CM2G that is constituted of the physical components described by Dunne et al. (2012). The atmosphere in this model, AM2, is identical to that employed in the Intergovernmental Panel on Climate Change (IPCC) Fourth Assessment Report (AR4) (Houghton et al. 2001) with a resolution of 2° latitude × 2.5° longitude and 24 vertical levels (Delworth et al. 2006). The primary difference between CM2G and CM2.1 is in the use of an isopycnal coordinate ocean model known as the Generalized Ocean Layer Dynamics (GOLD) model (Adcroft et al. 2008; Hallberg and Adcroft 2009). The ocean resolution is 1° in longitude, varies from 1° in latitude in the midlatitudes to 1/3° near the equator. The land model, LM3, is described by Shevliakova et al. (2009) and P. C. D. Milly et al. (2012, personal communication). The treatment of aerosols is identical to CM2.1, as described by Delworth et al. (2006). CM2 represents moist convection with the relaxed Arakawa–Schubert (RAS) formulation of Moorthi and Suarez (1992). Cloud microphysics are parameterized according to Rotstayn (1997) while mixed phased clouds are treated according to Rotstayn et al. (2000). Notably, the field of CCN is a prescribed two-dimensional field with a single value of 300 particles per cubic centimeter over land and 100 particles per cubic centimeter over ocean.

Earlier versions of CM2G have been used in a number of studies looking at the impact of regional changes in ocean color and upper-ocean mixing on the climate (Anderson et al. 2007; Harrison and Hallberg 2008). Gnanadesikan and Anderson (2009) found that the model has a cold bias in surface temperature and Anderson et al. (2009) show that it has a simulation of ENSO that is reasonably realistic. Like other models run with the AM2 atmosphere (Anderson et al. 2004), CM2G has weak tropical cyclone activity and weak tropical intraseasonal variability due to the Madden–Julian oscillation.

Several studies have compared precipitation patterns produced by earlier versions of the CM2 series to observed precipitation. In what follows we compare results from the tenth century of the CM2G 1860 control run to the corresponding run from CM2.1. Annual mean precipitation in CM2G is well correlated (>0.9) with CM2.1 which produced realistic precipitation patterns in the region around Indonesia, the belt of ITCZ rainfall north of the equator, and dry areas associated with subtropical high pressure systems (Dai 2006; Delworth et al. 2006). The seasonal migration of the ITCZ is also well represented in both models. While CM2G produces an erroneous double ITCZ, a common problem among global circulation models (Dai 2006; Delworth et al. 2006), the problem is less pronounced than in CM2.1. However, this improvement is somewhat offset by an enhancement of high precipitation biases relative to the Global Precipitation Climatology Project (GPCP) v2 data product (Adler et al. 2003) in the northern ITCZ and over Indonesia. Both models produce a relatively dry Amazon and predict somewhat more precipitation (12%–20%) than GPCP over the midlatitude regions where cloud whitening is applied in this study. The model performs slightly better when compared with the latest version of the CMAP Xie and Arkin (1997) dataset which has higher values of precipitation over the oceans as whole and about 6% higher values in the cloud-whitening regions.

Regional cool and dry ocean biases in CM2G (Gnanadesikan and Anderson 2009; Dai 2006) are both related to difficulties representing cloud fields in GCMs (Dai 2006). Karlsson et al. (1997) evaluated the marine subtropical cloud fields in nine models used in the IPCC Fourth Assessment Report. On average these models underestimated low clouds by 15% but overestimated shortwave reflectivity. A version of CM2.1 performed better than several other AR4 models, underestimating low clouds in the marine subtropics by 11%. CM2G shows a slight decline in marine low-cloud amount relative to CM2.1 (43.5% versus 44.2% globally and 29.9% versus 29.1% in the tropics). CM2.1 overestimated marine high clouds concurrently, but again showed a smaller bias than similar models. CM2G has essentially the same fraction of high cloud cover (34.5% globally). CM2.1 overestimated shortwave reflectivity similar to the other AR4 models, and CM2G reproduces this bias with essentially the same average tropical albedo of 25%. These biases are significant to this paper as the presence of fewer low clouds with greater albedo increases their susceptibility to cloud brightening. Unfortunately this is a persistent, pervasive problem in large-scale circulation models. Nevertheless, GCMs are a useful tool to examine global responses to a regional radiative forcing. The results presented in this paper focus on large-scale impacts for a given local forcing, rather than focusing on the specific cloud changes which are subject to documented biases.

b. *Experimental design*

Many different spatial distributions of cloud brightening could have been chosen, and each would produce a different climatic response. The present study seeks to emulate what a likely cloud-brightening distribution would look like. Similar to previous studies (Jones et al. 2009; Rasch et al. 2009), regions were selected in which low-level marine stratocumulous clouds are shown to persist throughout much of the year. These clouds have been judged to be the most susceptible to modification: they tend to have low values of naturally occurring CCN. Such clouds show the largest albedo response to a fixed addition of CCN (Bower et al. 2006).

We estimated the spatial extent of such low-level marine clouds from the International Satellite Cloud Climatology Project and additional estimates by other authors (Rossow and Schiffer 1991; Rossow and Schiffer 1999; Rozendaal et al. 1995). We restricted the geographic extent of cloud brightening to two large regions in the North Pacific and the Southern Ocean (boxed regions in Fig. 1) since Jones et al. (2009) identified these as the most effective regions to alter. We also sought to avoid a reduction in Amazonian

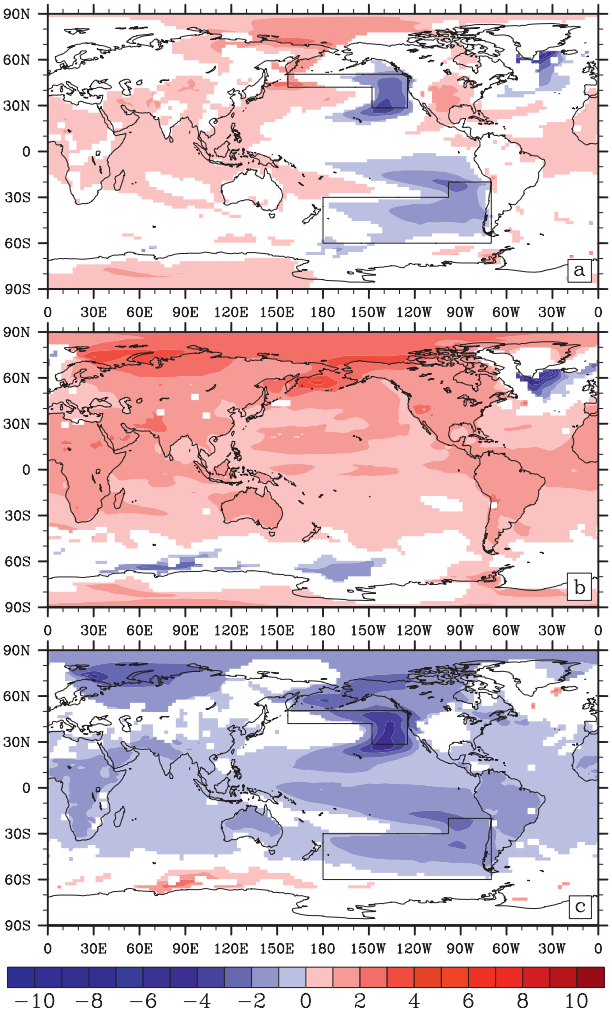

FIG. 1. Difference in surface temperature (°C), averaged over the first 40 years following cloud-brightening implementation, between the (a) GEO and PREIND simulations, (b) GW and PREIND simulations, and (c) GEO and GW simulations, statistically significant at 95% confidence level. White areas indicate insignificant differences.

precipitation observed by Jones et al. (2009) by not seeding the South Atlantic. Seeding was constant throughout time. We assumed the seeding scheme worked as envisaged, delivering the desired amount of droplets into the cloud base, and assumed these droplets were preferentially incorporated into cloud condensation nuclei as described by Bower et al. (2006). We did not attempt to address the cloud microphysical processes or other processes that are involved in the physical delivery mechanism.

Recent research by Korhonen et al. (2010) suggests that a large injection of droplets is required to overcome a microphysical feedback mechanism in which the injection of particles suppresses the in-cloud supersaturation and

prevents existing particles from forming cloud droplets. So the assumption that 1000 cm^{-3} of particles added to the cloud then becomes 1000 cm^{-3} CCN is likely an overestimate. The results will therefore represent a maximum, as previously discussed.

c. Model configurations

Three configurations of the model were used. The first experiment was a preindustrial control case (PREIND) was initialized and allowed to run for 300 years to provide a baseline against which to measure the changes from both anthropogenic greenhouse gases and cloud modification. The PREIND experiment had a static two dimensional field of CCN with a value of 300 cm^{-3} over the land and 100 cm^{-3} over the ocean. A second experiment represented anthropogenic gas emissions [global warming (GW)] with a CCN field that was identical to the PREIND case, and anthropogenic carbon dioxide that was increasing at a rate of 1% annually starting 40 years prior to the cloud-brightening perturbation to an eventual concentration of 4 times the preindustrial case after 140 years. A third experiment was the cloud-brightening geoengineering experiment (GEO). The trajectory of greenhouse gases was identical to the GW case. The field of CCN was modified such that the CCN value was instantly increased to 1000 cm^{-3} in the boxed regions of the North Pacific and Southern Ocean described above. This increase took place in the year 0 when the model was perturbed and was thereafter constant throughout the remainder of the simulation. The model timeline, with the accelerated +1% yr^{-1} CO_2 trajectory, can be roughly stretched to a more familiar scale, so that these experiments represent a world where cloud brightening is implemented in about 2025 when atmospheric CO_2 is 417 ppm. For each simulation, 140 years of model output were analyzed, a century longer than Jones et al. (2009) and 60 years longer than Rasch et al. (2009) in order to draw stronger inferences about temporally dependent responses.

Previous researchers have used various amounts of CCN to modify low-level marine clouds. Twomey theory predicts the change in shortwave reflectivity scales with the natural log of the fractional increase in CCN (Seinfeld and Pandis 1997; Merikanto et al. 2009; Korhonen et al. 2010) such that the albedo change due to adding particles flattens out as the number of particles increases. The difference between adding dissimilar but large amounts of CCN may be minimal. To explore this notion, an additional cloud-brightening experiment modified CCN to 500 cm^{-3} in the specified regions. This experiment was allowed to run for 100 years and was compared with the experiment with CCN set to 1000 cm^{-3}.

d. Analysis

Geoengineering via cloud modification has diverse effects on the whole climate system. Changes in ocean currents, deep water, seasonal ice extent, and other responses exist; some have been explored by other authors (Rasch et al. 2009; Jones et al. 2009). For brevity, the analyses presented here are restricted to surface temperature, precipitation, and effects associated with response of the Walker circulation.

Statistical analyses were performed on several scalar measures of the Walker circulation response in the following way to generate *p* values: An ordinary least squares fit was calculated for the anthropogenic warming experiment. This warming trend was removed from both the geoengineered (GEO) and anthropogenic (non-geoengineered) warming (GW) simulations to reduce variability due to greenhouse gases and retain cloud-brightening-induced variability. The values were resampled with replacement 10 000 times to generate sampling distributions of the median of each variable. The actual GEO 140-yr median was then compared with the sampling distribution of the GW values to determine how unusual the GEO value was compared with the potential GW values, providing a nonparametric significance test.

4. Results

a. Surface temperature

In the first 40 years of the cloud-brightening perturbation, the surface temperature in many regions is statistically indistinguishable from preindustrial conditions (Fig. 1a). The global average difference between the GEO and PREIND surface temperature is +0.16°C, compared with a +1.03°C difference in the GW scenario. The regions directly affected by cloud seeding exhibit a net cooling of 0°–4°C, while the northern polar latitudes show a net warming of 0°–4°C. For context, the warming under the GW scenario (without cloud brightening) was considerably larger during the same 40-yr period (Fig. 1b). The northern latitudes are warmed 3°–6°C and most continental regions are 1°–4°C warmer than PREIND.

Figure 1c shows the difference between the GEO and GW simulations, that is, the linear effect of cloud brightening. Most of the globe is cooled due to cloud brightening, with a global average of −0.96°C. The strongest cooling occurs in the regions of modified cloud albedo and in the northern latitudes (Fig. 1c).

Seasonal averages of the GEO–GW temperature differences are shown for the first 40 years (Fig. 2). Globally averaged, the cooling effect of cloud brightening was −1.1°C in September–November (SON) and

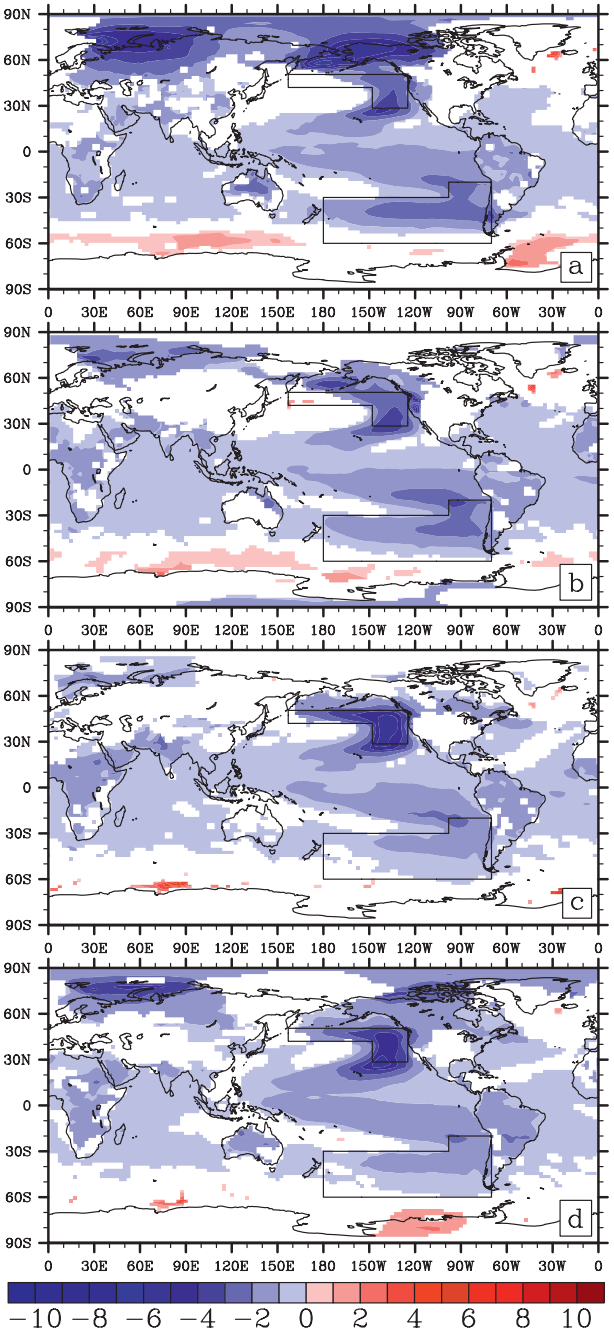

FIG. 2. Seasonal differences in surface temperature (°C), averaged over the first 40 years following cloud-brightening implementation, between the GEO and GW simulations, statistically significant at 95% confidence level: (a) DJF, (b) MAM, (c) JJA, and (d) SON. White areas indicate insignificant differences.

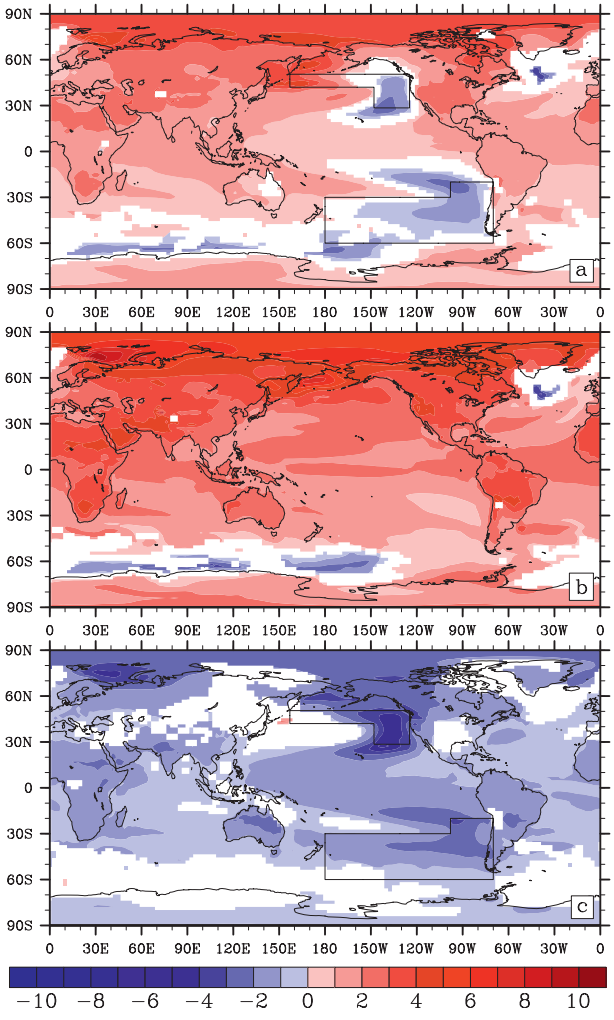

FIG. 3. Difference in surface temperature (°C), averaged over 140 years following cloud-brightening implementation, between the (a) GEO and PREIND simulations, (b) GW and PREIND simulations, and (c) GEO and GW simulations, statistically significant at 95% confidence level. White areas indicate insignificant differences.

December–February (DJF) compared with −0.92°C in March–May (MAM) and June–August (JJA). However, the extent of cooling was greater for boreal winter. Suppression of warming in the high northern latitudes was concentrated in boreal winter; Arctic surface temperature in boreal spring and summer were statistically no different than under the GW simulation. The modified region in the Northern Pacific was cooled throughout the year, whereas the Southern Ocean modified region experienced the strongest cooling during the boreal winter and spring. Continental landmasses also cooled primarily during boreal winter, although in the Southern Hemisphere a temperature signal persisted throughout the year. Over 140 years (not shown) the seasonal temperature response was spatially similar albeit with larger cooling in the Arctic during boreal autumn and winter.

In the 140-yr mean, the effect of cloud brightening (GEO − GW) demonstrates a similar spatial pattern to the first 40 years. Globally averaged temperature with

geoengineering was 1.28°C cooler than without cloud brightening. The strongest cooling occurs in the brightened zones (1°–4°C) and the northern polar latitudes (3°–4°C) (Fig. 3c). The continents experience greater cooling on average (2°–5°C) relative to the first 40 years, mainly because the magnitude of warming due to GHGs is much larger over the longer time period (Fig. 3b). The global mean temperature increases 3.6°C under GW (Fig. 3b) compared with 2.0°C under GEO (Fig. 3a). Relative to preindustrial conditions, the GEO experiment shows a pronounced warming in the midwestern United States where the cloud brightening has a diminished cooling effect (Fig. 3a). Temperatures in the midwestern United States are indistinguishable between the GEO and GW experiments (Fig. 3c).

b. Surface precipitation

The precipitation signal was considerably noisier than the temperature signal. Only the strongest signals appeared in the 40-yr mean; the availability of 140 years of model output allows more extensive analysis. The most striking precipitation response occurred in the eastern equatorial Pacific. In the first 40 years, precipitation increased under cloud brightening by nearly a meter annually in Indonesia, and decreased by a similar magnitude in the adjacent Pacific Ocean (Fig. 4a). For context, these changes are occurring in a region whose average annual rainfall from 1979–2002 was 2.0–2.5 m (Adler et al. 2003). There was an insignificant Pacific equatorial precipitation response in the GW simulation in the first 40 years. Over 140 years, the equatorial Pacific signal includes a small increase from the effects of anthropogenic GHGs (~30 cm yr^{-1}, Fig. 5b) and a larger increase due to cloud brightening alone (70–90 cm yr^{-1}, Fig. 5c). In the 140-yr mean, precipitation in the equatorial Pacific changed by more than a meter due to cloud brightening; rainfall increased over Indonesia and declined over the adjacent Pacific Ocean.

Averaged over 140 years of simulation, the global average annual precipitation increases from the preindustrial run by 2.85 cm in the GW case (Fig. 5b) and decreases by 0.53 cm in the GEO case (Fig. 5a). Relative to the preindustrial, cloud brightening caused a 0–5 cm yr^{-1} decline in precipitation in the midwestern United States (Fig. 5a) associated with the anomalous warming in the region. Cloud brightening induced additional rainfall in the Sahel (Fig. 5c), which helped compensate for the drying observed in the GW experiment (Fig. 5b) with the net impact of cloud brightening with increased greenhouse gases nearly unchanged from preindustrial conditions (Fig. 5a). We observe a small (0–10 cm yr^{-1}) increase in the Amazon, consistent with the results of Rasch et al. (2009) and with Jones et al. (2009) when the clouds in the southern Atlantic were not brightened (Fig. 5a); however, the Amazon precipitation response was not significantly different between the GEO and GW experiments at a 95% confidence level (although it was significant at 90%).

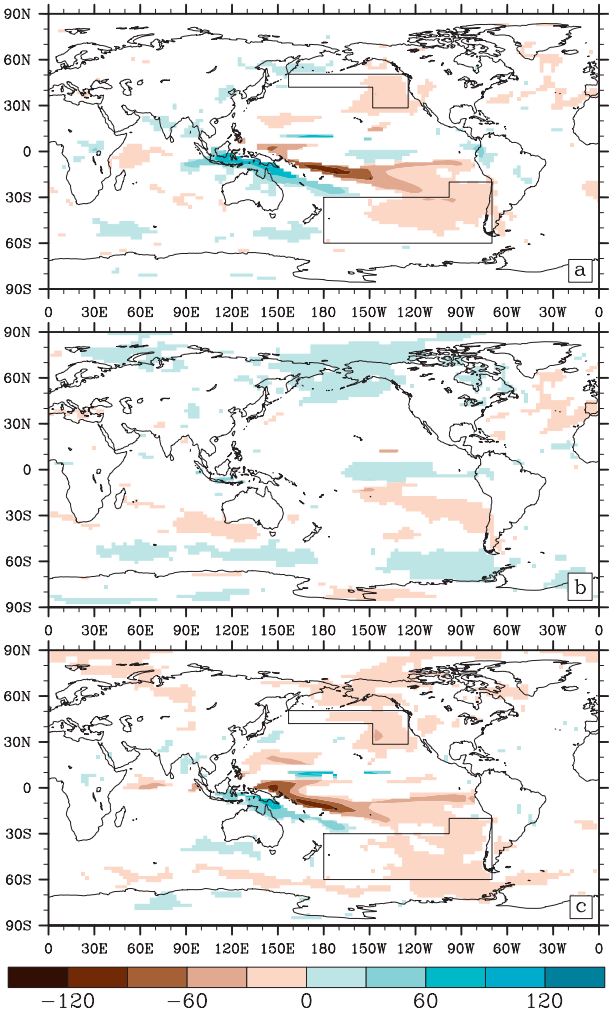

FIG. 4. Difference in total annual precipitation (cm yr^{-1}), averaged over first 40 years following cloud-brightening implementation, between the (a) GEO and PREIND simulations, (b) GW and PREIND simulations, and (c) GEO and GW simulations, statistically significant at 95% confidence level. White areas indicate insignificant differences.

Seasonal averages of the difference in precipitation over 140 years are shown in Fig. 6. Globally averaged GEO − GW precipitation was −5.7 cm during boreal winter and spring, and −3.9 cm during boreal summer and autumn. The precipitation couplet in the eastern equatorial Pacific is present throughout the year, with a minimum magnitude in MAM. During SON the Indonesian increase is somewhat stronger whereas the oceanic decline dominates during DJF. Precipitation in

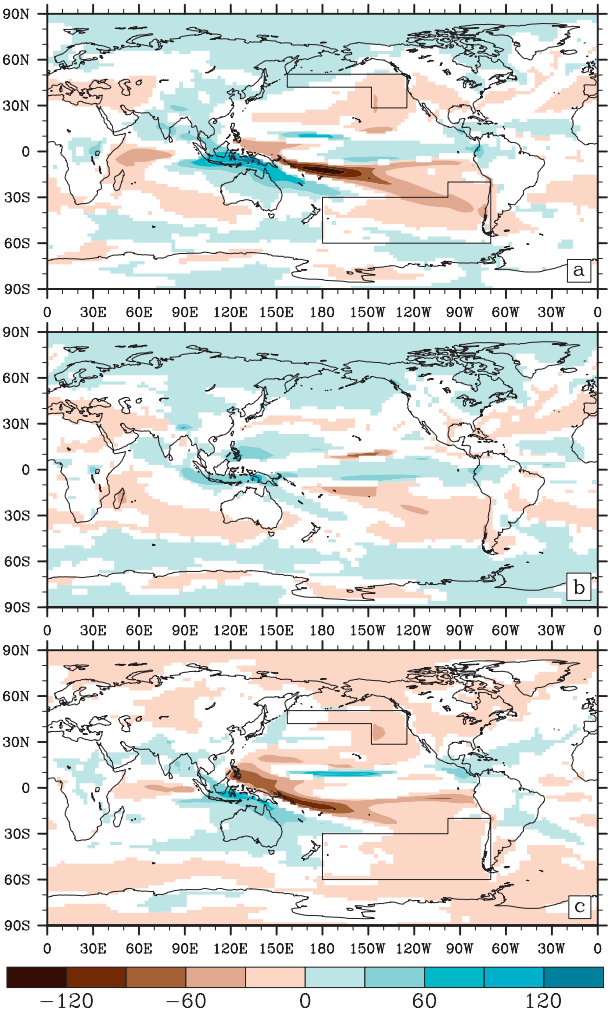

FIG. 5. Difference in total annual precipitation (cm yr^{-1}), averaged over 140 years following cloud-brightening implementation, between the (a) GEO and PREIND simulations, (b) GW and PREIND simulations, and (c) GEO and GW simulations, statistically significant at 95% confidence level. White areas indicate insignificant differences.

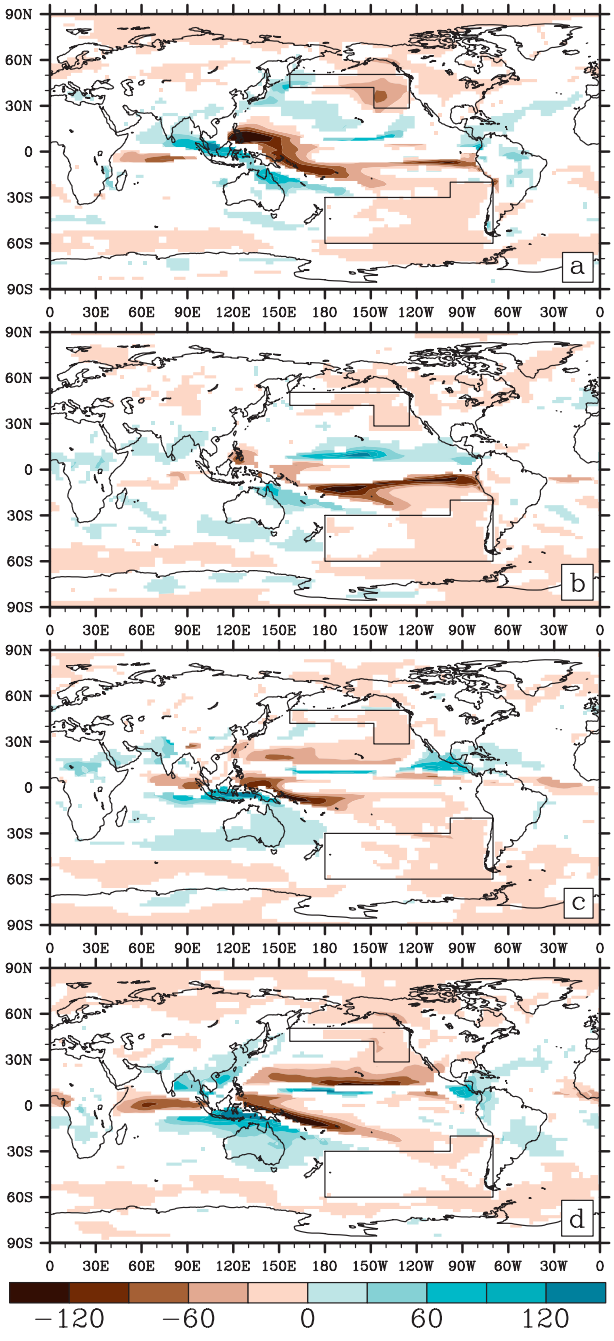

FIG. 6. Seasonal differences in total precipitation (cm yr^{-1}), averaged over 140 years following cloud-brightening implementation, between the GEO and GW simulations, statistically significant at 95% confidence level: (a) DJF, (b) MAM, (c) JJA, and (d) SON. White areas indicate insignificant differences.

the Sahel region is enhanced during the boreal spring and summer. Interestingly, GW rainfall exceeds GEO rainfall over the central Pacific south of the equator during MAM while GEO rainfall exceeds GW rainfall in this region during SON. This suggests an intertropical convergence zone that moves less strongly or more slowly away from the equator in the summer hemisphere because of cloud brightening.

The spatial response in surface precipitation emerged in the first 20 years of the GEO simulation and persisted throughout the model run. Rasch et al. (2009) demonstrated a similar magnitude increase in Indonesian precipitation with an adjacent decrease using CCSM3 but did not investigate the feature further. We investigated the precipitation response in detail and found a significant response in the Walker circulation. We found associated changes in hurricane potential, sea surface temperature, and vertical wind shear. The remainder of this analysis will explore these results.

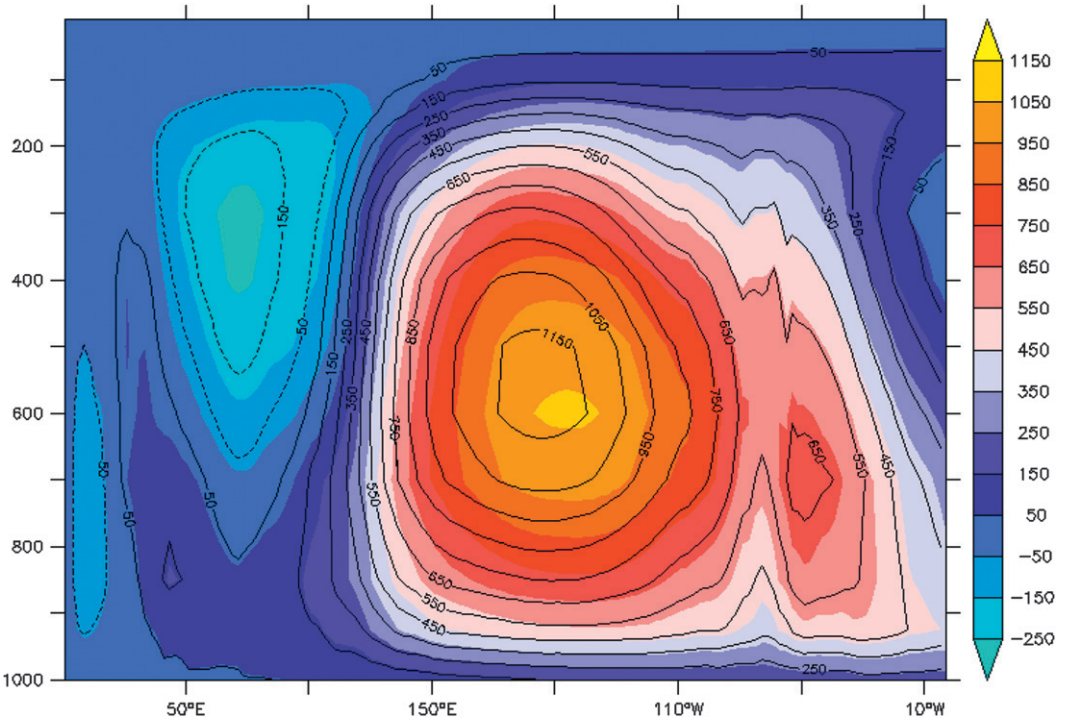

FIG. 7. Vertical cross section of the meridional mass streamfunction (10^9 kg s^{-1}), showing the Walker circulation. Magnitudes have been negated such that positive values represent normal clockwise circulation. Black contours are the streamfunction for the GEO simulation. Shaded contours are the streamfunction for the GW simulation. Averaged over 140 years following cloud-brightening implementation.

c. *Walker circulation*

Previous studies have shown an eastward shift in the Walker cell associated with positive sea surface temperature anomalies in the Pacific Ocean under increasing CO_2 simulations (Roeckner et al. 1999). We investigated whether increasing the albedo of Pacific marine stratus clouds would have an opposite effect. Do the induced negative SST anomalies in the Pacific (Fig. 3c) coexist with a westward shift in the Walker circulation?

The precipitation pattern suggested a westward (e.g., toward Indonesia) shift and intensification in the ascending branch of the Walker circulation. Figure 7 shows a vertical cross-section of the mass streamfunction averaged along meridians between 30°S and 30°N annually averaged over 140 years following the cloud-brightening perturbation. The sign has been reversed such that the primary clockwise flow is shown with positive values. The shift in the Walker circulation is here clearly visible. Shaded values show the mean circulation in the GW simulation, while black contours show the mean circulation in the GEO experiment. The central maximum is shifted 8.2° to the west and has increased because of cloud brightening from 1100×10^9 to 1178×10^9 kg s^{-1} (Fig. 7). The western branch of ascent has undergone a similar longitudinal shift toward Indonesia (Fig. 7), which helps explain the large precipitation changes observed in this region (Fig. 5c).

The nonparametric resampling and parametric test was performed on two scalar measures of the Walker circulation, its central maximum magnitude and the longitude at which the maximum occurred. During the first third of the simulation, the central longitude distribution is located approximately 7° to the west under GEO compared with GW ($p < 0.05$). During the second third, the westward separation is approximately 5° ($p < 0.05$). As the GEO central longitude drifted westward, the GW did not vary significantly; hence the separation between the two distributions was due primarily to geoengineering. During the final third of the simulation, the medians of each distribution are not statistically different ($p = 0.15$) as the increasing warming effects of anthropogenic CO_2 overcome the cooling effect of cloud modification.

The Walker central magnitudes were resampled in the same way. In each time period, the sampling distribution of the medians were shifted to higher magnitudes under GEO compared with the GW experiment, showing an increase in the strength of the Walker circulation under cloud brightening. During the first third of the

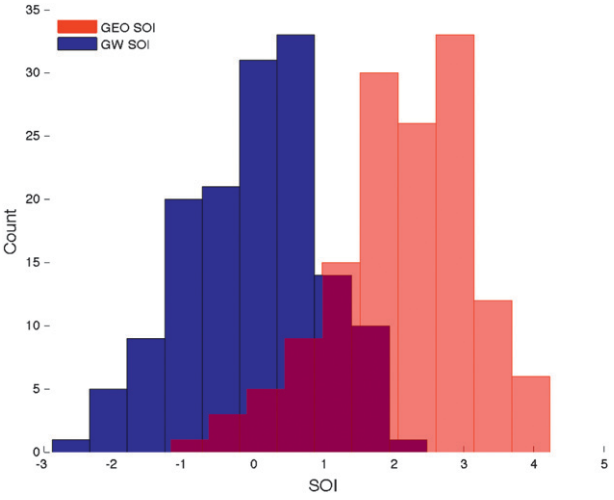

FIG. 8. Southern Oscillation index annual values in GW and GEO over 140 years. GEO values are computed as the Tahiti–Darwin pressure difference, normalized by the GW difference and std dev from the month. GW SOI is computed as the difference normalized by itself.

simulation following the cloud-brightening perturbation, the center of the GEO distribution is approximately 50×10^9 kg s^{-1} larger than the center of the GW distribution ($p < 0.05$). During the second third of the analysis, the GEO values are approximately 80×10^9 kg s^{-1} greater ($p < 0.05$). During the final third of the simulation, the GEO distribution is 100×10^9 kg s^{-1} greater than GW ($p < 0.05$). Hence, with the GW trend removed, the Walker circulation is intensified under cloud brightening relative to the global warming without cloud brightening. This intensification seems to increase in time as the GEO magnitudes remain fairly stationary and the GW distribution drifts toward lower values.

Thus we find that in these simulations, the Walker circulation is shifted to the west and intensified when cloud brightening is in place versus when it is not. The increase in magnitude is more consistent than the change in longitude, in part because the detrended longitude sampling distribution is relatively broad in the GW simulation. These results are consistent with the modeled changes in precipitation in the equatorial Pacific.

d. Southern Oscillation index

To further characterize the atmospheric response to cloud brightening, we plotted histograms of the Southern Oscillation index (SOI) at each year in the GW and GEO experiments (Fig. 8). SOI values were calculated on annual averages of sea level pressure. For the GW data, SOI was computed as the standardized anomaly of the SLP difference between Tahiti and Darwin, in the usual way. For the GEO data, SOI was calculated as the SLP difference between Tahiti and Darwin in the GEO case, which was then standardized by the GW mean and standard deviation which were calculated for 140 years. This enables us to compare the two computed indices directly. A very high GEO SOI represents a strong cool ENSO phase relative to the GW scenario, whereas a very low GEO SOI represents a strong warm ENSO phase relative to the GW scenario. Figure 8 shows the distribution of the SOI under the GEO and GW experiments. The GEO simulation has large positive values of SOI for most years; only a few years have negative SOI, whereas the GW distribution is centered at zero by definition. For context, in the real atmosphere the range of SOI is usually -3.0 to $+3.0$ at the extremes. So by implementing cloud brightening, we have inadvertently induced a fairly strong, permanent "La Niña" signal in the Southern Oscillation index. This is consistent with our results from examining the Walker circulation. The following analyses show a related signal: enhanced hurricane potential in the Atlantic Ocean.

e. Tropical cyclogenesis

Our simulations were run at too coarse resolution to resolve individual storm signatures, so we estimated the characteristics of tropical cyclogenesis in the Pacific and Atlantic Basins using grid-scale parameters, bearing in mind that our results speak to theoretical potential storms rather than actual simulations of individual tropical cyclones. These values are calculated on the Atlantic hurricane season (June–November) during the first 20 years after cloud brightening is implemented. We present results for maximum potential intensity (MPI), vertical wind shear, and genesis potential index.

Figure 9a shows the difference (GEO − GW) of MPI averaged over July–November during the first 40 years of the cloud-brightening perturbation. Cloud brightening is associated with large changes in MPI over the northeastern extratropical Pacific, but largely in regions where tropical cyclones do not form. A 1–4 m s^{-1} increase in MPI is seen across a large portion of the tropical Atlantic (10°–20°N), comprising a roughly a 5% increase in a region of frequent cyclogenesis in the current climate. MPI was strongly suppressed in the cloud modification region by 10–25 and 4–8 m s^{-1} in the central Pacific. MPI rose off the eastern coast of Japan and in the South China Sea by 2–4 m s^{-1}.

1) VERTICAL WIND SHEAR

Lower values of vertical wind shear are conducive to hurricane formation and intensification (Palmer 2002; Goldenberg et al. 2001). During the hurricane season, vertical wind shear must be less than 12.5–15 m s^{-1} in order for a tropical cyclone to develop (McBride and

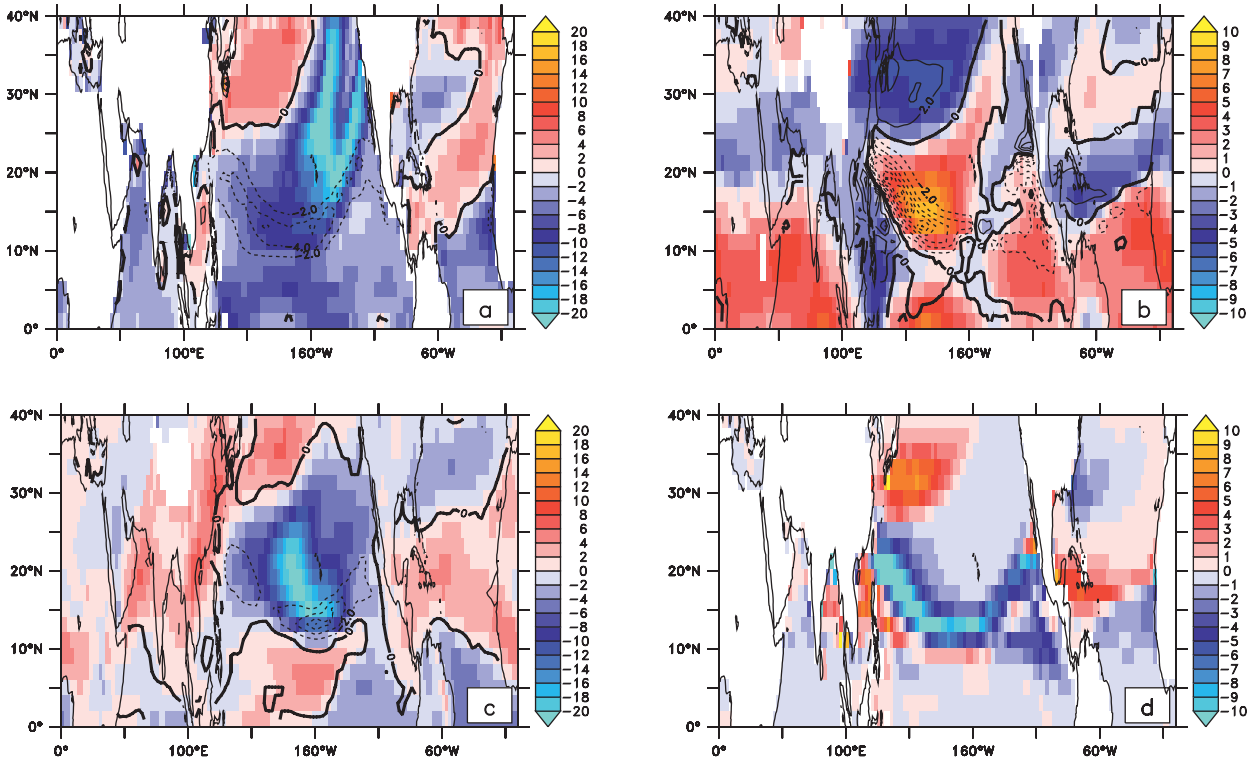

FIG. 9. Hurricane-season (June–November, first 20 years following cloud-brightening implementation) average (a) maximum potential hurricane intensity (m s^{-1}), (b) relative humidity, (c) vertical wind shear, (m s^{-1}), and (d) genesis potential index. Difference between GEO–GW simulations.

Zehr 1981; Frank and Ritchie 2001). A difference of 2–5 m s^{-1} can determine whether a cyclone will form, intensify, or decay (Palmer 2002). We investigated the wind shear response to cloud brightening to explore its relationship to hurricane intensity.

We computed average hurricane season 850–200-mb vertical wind shear (magnitude):

$$\text{Shear} = |\mathbf{V}(200\,\text{mb}) - \mathbf{V}(850\,\text{mb})| \qquad (1)$$

over the tropical Atlantic and Pacific during the hurricane season for the first 20 years after cloud brightening began. Figure 9b is a regional map of the change in wind shear due to cloud brightening. In the Atlantic, vertical wind shear was greater in the cloud brightening simulation by 1–3 m s^{-1} between 5° and 10°N, which would contribute to decreased tropical cyclone formation in the lower tropics. However, vertical wind shear declined by 3–4 m s^{-1} in the Caribbean Sea, potentially enhancing cyclogenesis in this vulnerable region. Vertical wind shear increased by 2–3 m s^{-1} in the Pacific near Central America and by more than 5 m s^{-1} across much of the tropical Pacific, but decreased by 2–5 m s^{-1} in the South China Sea, in the eastern Pacific near Indonesia, and off Japan.

2) GENESIS POTENTIAL INDEX

The genesis potential index (GPI) developed by Emanuel and Nolan (2004) and described by Camargo et al. (2007a) attempts to predict frequency of cyclone formation from large-scale environmental parameters. GPI is an empirically derived measure which has been shown to perform fairly well over multidecadal time scales in several oceanic basins (Camargo et al. 2007a,b). The index is computed as follows (from Camargo et al. 2007a):

$$\text{GPI} = |10^5\eta|^{3/2}\left(\frac{H}{50}\right)^3\left(\frac{V_{\text{pot}}}{70}\right)^3(1 + 0.1V_{\text{shear}})^{-2} \qquad (2)$$

where η is the absolute vorticity at 850 mb, H is the relative humidity at 600 mb, V_{pot} is the potential intensity, and V_{shear} is the magnitude of the 850–200-mb vertical wind shear. GPI thus drops as shear increases, as midatmosphere relative humidity decreases, and as the absolute vorticity decreases. GPI is a measure of how

many tropical cyclones might be expected to develop in a 5° box per decade, with values peaking over 20 in the northwestern tropical Pacific, the most active region for the development of tropical cyclones. Much lower values (~5–8) are found in the Atlantic basin. As noted by Gnanadesikan et al. (2010) GPI in the CM2G model is biased toward predicting typhoon generation too close to the equator relative to observations. Its use here should thus be taken as a rough scaling for the potential impact of cloud brightening on regional cyclogenesis, suggesting where future work may be required.

Changes in GPI can be used to estimate the impact of changes in shear and MPI described above on tropical cyclone activity. By changing one variable at a time, one can isolate different mechanisms for cloud whitening to produce changes in tropical cyclone activity. The contours in Figs. 9a,b,c show the changes in GPI in the cloud-brightening simulation relative to the global warming case that are associated with the changes in MPI, shear, and midtropospheric relative humidity, respectively. Note that while MPI shows large decreases in midlatitudes, GPI decreases associated with these changes are concentrated in the tropics, as the central gyres tend not to generate many tropical cyclones. The changes in MPI produce a decline in GPI over the Pacific, with essentially no impact in the Atlantic basin. In the region from 150°E to 150°W and 10°–15°N, GPI during the July–November period nearly doubles from 8.7 to 13.8 under global warming, but drops as a result of the MPI changes to 9.5.

Changes in the shear reinforce the MPI changes where they produce significant declines in the North Pacific. Over the region just mentioned, the shear change results in a drop in GPI to 9.6, equivalent to the change from MPI but with much larger drops to the north and west. However, the shear changes also result in increases in other regions, such as off Japan and in the Caribbean. The impact on GPI of relative humidity changes is smaller than that associated with MPI and shear and is limited to the northeastern Pacific. Vorticity changes (not shown) have a relatively minor overall impact.

The total GPI change (Fig. 9d) shows a large decrease along the edge of the Pacific subtropical high, which essentially cancels an increase of similar magnitude under global warming. Off Japan, however, the region from 30° to 40°N and 140° to 160°E sees a decrease from 3.5 to 2.6 under global warming, but an increase to 6.5 with cloud whitening. In the Atlantic, the region from 15°–25°N and 100°–50°W sees essentially no change under global warming, but increases from around 4.2 to 6.7 (a more than 50% increase) under cloud whitening.

The magnitude of changes we see here is consistent with the changes seen across many models by Vecchi and Soden (2007). The pattern of change is consistent with the hypothesis of Vecchi et al. (2008) that cyclogenesis depends not on the absolute value of SST locally but on its value relative to the tropical mean. Our results suggest that it will be important to include dynamical downscaling studies for cyclogenesis such as those carried out by Knutson et al. (2008) in any full evaluation proposed geoengineering strategies that modify patterns of tropical temperatures and atmospheric circulation.

f. *Difference in response between 1000 and 500 cm^{-3} CCN experiments*

The susceptibility of cloud shortwave reflectivity α_c to fractional changes in cloud drop number concentration N is inversely proportional to N such that when N is high, cloud reflectivity is less sensitive to changes in N. This relationship is described by (Twomey 1991; Platnick and Twomey 1994; Seinfeld and Pandis 1997)

$$\Delta\alpha_c = \frac{1}{3}[\alpha_c(1-\alpha_c)]\Delta \ln(N), \tag{3}$$

provided the liquid water path is maintained. A second cloud-brightening simulation was performed over 125 years in order to explore the climate and tropical circulation response to modifying the CCN of the marine stratus deck regions to 500 cm^{-3}. Cloud shortwave reflectivity in the modified regions peaked at 0.44 in both cloud-brightening experiments. Liquid water path was likewise unchanged by virtue of the model specifications. For $\alpha_c = 0.44$, $N_1 = 500$ cm^{-3}, and $N_2 = 1000$ cm^{-3}, Eq. (3) predicts a change in cloud shortwave reflectivity of 0.057 because of the doubling of CCN from 500 to 1000 cm^{-3}, a 13% increase. The attendant differences in climate and atmospheric circulation are expected to be moderate.

The model simulation with 1000 cm^{-3} was compared with the simulation with 500 cm^{-3}. Surface precipitation and temperature were examined on an annual and seasonal basis for 100 years. Annual averages of the maximum magnitude and central longitude of the Walker circulation were also considered for 140 years. For brevity, the results of this analysis are summarized in Table 1.

For each variable, the time series were bootstrapped with replacement 10 000 times to construct nonparametric distributions of the data. This method allows side-by-side comparison amongst sample variables with different underlying distributions. The sample means and 95% confidence intervals are reported in Table 1.

In general the results confirm the prediction that fractional changes in CCN do not induce physically significantly different responses when CCN is already

TABLE 1. Global averages of the differences of several variables in the 1000 cm^{-3} CCN, 500 cm^{-3} CCN, and preindustrial experiments, with their 95% confidence intervals.

	GW − PREIND	GW1000 − PREIND	GW1000 − CW500
Walker central latitude (°E)	−4.45 ± −3.36	−7.58 ± −3.51	0.56 ± −2.64
Walker central magnitude (10^9 kg s^{-1})	−5.30 ± −1.80	14.9 ± 1.80	0.40 ± 1.80
Annual mean global temperature (K)	1.66 ± −0.14	0.72 ± −0.11	−0.14 ± −0.03
JFM mean global temperature (K)	1.68 ± −0.15	0.67 ± −0.12	−0.13 ± −0.04
AMJ mean global temperature (K)	1.55 ± −0.13	0.68 ± −0.10	−0.14 ± −0.03
JAS mean global temperature (K)	1.60 ± −0.13	0.73 ± −0.11	−0.16 ± −0.03
OND mean global temperature (K)	1.84 ± −0.16	0.81 ± −0.12	−0.15 ± −0.04
Annual mean global precipitation (cm yr^{-1})	16.4 ± −1.4	−6.2 ± −1.3	−2.6 ± −0.8
JFM mean global precipitation (cm yr^{-1})	22.3 ± −2.2	−4.8 ± −1.9	−1.9 ± −1.2
AMJ mean global precipitation (cm yr^{-1})	15.3 ± −1.7	−7.8 ± −1.6	−4.0 ± −1.4
JAS mean global precipitation (cm yr^{-1})	13.5 ± −1.8	−6.6 ± −1.8	−1.4 ± −1.3
OND mean global precipitation (cm yr^{-1})	16.6 ± −1.6	−5.7 ± −1.6	−3.2 ± −1.3

high. Seasonal and annual mean surface temperatures are somewhat higher in the 500 cm^{-3} CCN experiment, but the differences are small relative to the cooling induced by cloud brightening at the 1000 cm^{-3} CCN level. Figure 10 shows the seasonal average differences in temperature and confirms the differences are an order of magnitude smaller than those associated with GEO. Surface precipitation is slightly lower in the 1000 cm^{-3}; these differences are greater for boreal spring and autumn. The regions where one brightening experiment differed from the other in precipitation coincide with the regions affected by cloud brightening (Fig. 11) The somewhat lower values of precipitation in the 1000 cm^{-3} experiment are due to greater drying over the equatorial Pacific Ocean during boreal spring and autumn. The differences in precipitation between the two cloud brightening experiments are half as small in magnitude as the drying due to cloud brightening alone and considerably smaller than the precipitation changes in the anthropogenic warming scenario. The central magnitude and longitude of the Walker circulation are indistinguishable between the 1000 and 500 cm^{-3} CCN experiments, with mean differences straddling zero. These results suggest temperature and precipitation responses are slightly more sensitive to fractional changes in model CCN than tropical circulation, but otherwise the effects of cloud brightening do not differ strongly between the 500 and 1000 cm^{-3} simulations.

5. Discussion

Our study emphasizes the complexity of the climatic response to a given geoengineering strategy. We chose to simulate an enhancement of marine stratocumulus clouds because this option has been advocated by various authors, and previous authors have examined the potential of this kind of geoengineering to compensate for the effects of anthropogenic climate change (Latham et al. 2008; Jones et al. 2009; Rasch et al. 2009). Our investigation has shown that the implementation of a cloud-brightening scheme of adequate scale to counteract some impacts of quadrupled CO_2 would engender a complex response in the global climate system. Moreover, our study shows that the cooling afforded is probably still insufficient to counteract the effects of greenhouse gas emissions, particularly over longer time scales.

The results from our temperature analysis are reasonably consistent with previous research. By brightening clouds over 20% of the ocean, Rasch et al. (2009) were able to modify the simulated climate to produce a 0°–4°C cooling in their cloud-brightened regions, 0°–3°C warming over most continents, 0°–1°C warming over the oceans, and a 2°–4°C warming over the Arctic (all relative to preindustrial conditions). Jones et al. (2009) simulated a cloud-brightened temperature pattern with similar features: 0°–1°C cooling over the brightened regions, 0.5°–2.5°C continental warming, 0°–1°C ocean warming, 2°–3°C Arctic warming (all relative to preindustrial conditions). Using a scheme that brightened roughly 15% of oceanic clouds, similar to Rasch et al. (2009) and Jones et al. (2009) our results were consistent with these studies. We explored the seasonal response in surface temperature and found much of the Arctic cooling was concentrated in the boreal winter, where it would likely contribute to ice pack but may not slow summer ablation rates. This result supports the finding by Rasch et al. (2009) that Arctic sea ice may respond favorably to cloud brightening.

The degree of similarity between these three studies suggest the surface temperature response is not very sensitive to the inclusion of the South Atlantic [as in Jones et al. (2009)] or temporally variable albedo enhancement [as in Rasch et al. (2009)] so long as the North and South Pacific are modified.

The similarity between these studies also suggests the cooling response is not very sensitive to the amount of

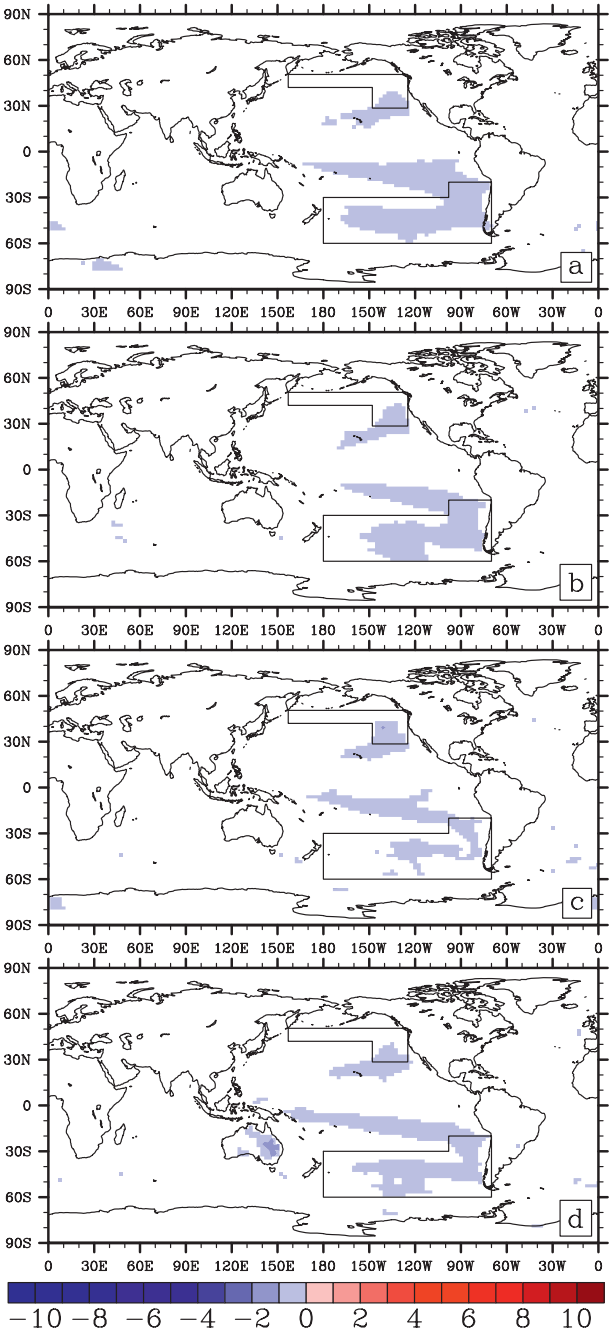

FIG. 10. Seasonal differences in surface temperature (°C), averaged over 125 years following cloud-brightening implementation, between the 1000 and 500 cm^{-3} cloud-brightening simulations, statistically significant at 95% confidence level: (a) January–March (JFM), (b) April–June (AMJ), (c) July–September (JAS), and (d) October–December (OND). White areas indicate insignificant differences.

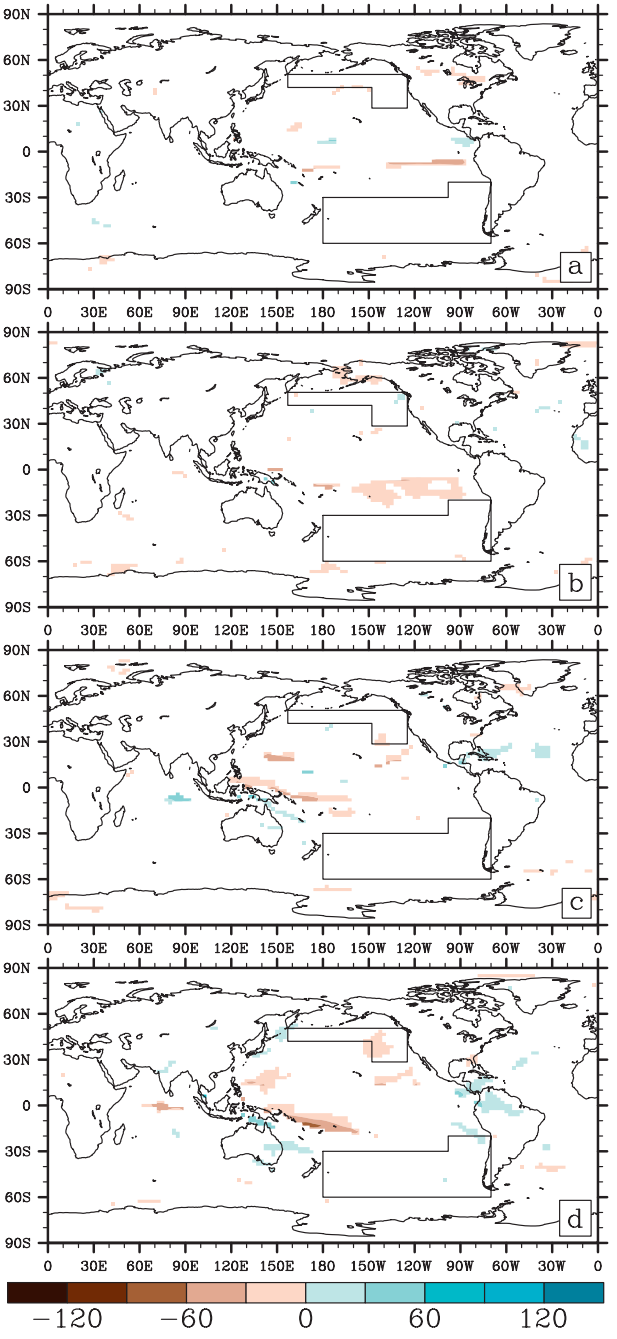

FIG. 11. Seasonal differences in surface precipitation (cm yr^{-1}), averaged over 125 years following cloud-brightening implementation, between the 1000 and 500 cm^{-3} cloud-brightening simulations, statistically significant at 95% confidence level: (a) JFM, (b) AMJ, (c) JAS, and (d) OND. White areas indicate insignificant differences.

CCN artificially "added" to stratus cloud decks. The present study was the first to examine cloud brightening at two different CCN thresholds within the same modeling framework. We observed similar responses at 500 as 1000 cm^{-3}. This is unsurprising as the bulk radiative cloud properties in large-scale models imply weak sensitivity of cloud albedo to CCN at higher values of CCN. According to these principles, the threshold for

temperature modulation may be closer to the 375 cm^{-3} used by Jones et al. (2009) than the 1000 cm^{-3} used by Rasch et al. (2009) and the present study. The data suggested the tropical circulation response at 500 cm^{-3} CCN is not significantly enhanced at 1000 cm^{-3} CCN, while precipitation and temperature are slightly more sensitive to increasing CCN. The robustness of this result depends strongly on the interaction of marine clouds and aerosols, which are not well simulated by large-scale models. Future research should investigate the sensitivity in response to fractional changes in CCN using observations and large-eddy simulations better suited to the task.

Even assuming perfect efficacy, each of the three studies considered here were unable to achieve full amelioration of the temperature increase under increasing CO_2. This was true for the first few decades in each study, but particularly for a longer time period in the present work. This was true for an AIB trajectory (Jones et al. 2009), $2 \times CO_2$ (Rasch et al. 2009), and $4 \times CO_2$ (present paper). Despite significant initial cooling effects each study demonstrated continued Arctic warming of 2°–4°C.

Our precipitation results agree moderately well with those of Rasch et al. (2009) and agree overall very well with the 0.7–1.1 m yr^{-1} increase in Indonesian rainfall observed in both studies. Jones et al. (2009) lacked such a response, perhaps because the extent and degree of cloud-brightened cooling in the North Pacific was smaller. The precipitation response under cloud brightening seems to be more sensitive than the temperature response to variations in the regions brightened and the change in CCN chosen, a point already made by Rasch et al. (2009). Neither Rasch et al. (2009) nor the present study observed negative rainfall departures in South America, further supporting the conclusion by Jones et al. (2009) that cloud modification in the South Atlantic caused Amazonian rain decrease in that study.

We concur with Jones et al. (2009) and Rasch et al. (2009) that cloud-brightening geoengineering would likely have winners and losers in rainfall. Ultimately though, the relative effects of any cloud-brightening scheme depend on the climate response to warming. For example, Rasch et al. (2009), Jones et al. (2009), and the present study demonstrated +0–20 cm yr^{-1} rainfall changes from preindustrial due to cloud brightening in the Sahel region of Africa; our work found these increases during the agricultural season. However, these small annual increases were overwhelmed by CO_2-induced drying in the $2 \times CO_2$ and $4 \times CO_2$ cases (Rasch et al. 2009; present study) but not in the A1B trajectory (Jones et al. 2009). Thus our ability to assess the impacts of cloud brightening is only as good as our ability to simulate the future climate without cloud brightening.

The present study advanced beyond previous research by investigating the dynamic response associated with the surface precipitation. We discovered a westward shift and intensification in the Walker circulation, an increase in the Southern Oscillation index, and an increase in maximum potential hurricane intensity and genesis potential index in the Atlantic Ocean and South China Sea in response to cloud brightening. We argued that the change in MPI and GPI were promoted by a decrease in 850–200-mb vertical wind shear. These changes occurred during the tropical hurricane season and may influence hurricane formation and intensity. Future research should explore these responses at higher spatial resolutions.

This paper examined the difference in responses between 500 and 1000 cm^{-3} using the same model, anthropogenic gas trajectory, and regional pattern of cloud modifications, adding a dimension lacking in previous work. Our results show the surface and tropical circulation effects of 500 and 1000 cm^{-3} are similar. We might therefore expect changes in circulation in simulations which used lower but still artificially high values of CCN. It would also be worthwhile to reexamine the simulations in Rasch et al. (2009) to see if their precipitation response was a signal of changes in the Walker circulation. In addition, one could ask if there is a threshold, whether in the change in CCN or areal extant of cloud brightening, above which a circulation response is evident. Jones et al. (2009) saw no such response at 375 cm^{-3}. Would their methods induce a response at 500 or 1000 cm^{-3}?

Cloud brightening is like any geoengineering in that its primary goal is to moderate surface temperature. Such moderation is theoretically possible, albeit imperfect, including continued warming and enhanced Arctic warming. But in the process of cooling the surface, we risk introducing a complex dynamical response with uncertain and potentially dramatic results. There are many unknowns, and we urge future researchers to consider the immediate and long-term responses of the whole climate system.

Acknowledgments. I am heartily grateful to my research advisers, Anand Gnanadesikan and Art DeGaetano, each of whom provided invaluable support throughout the course of this research. I thank Bonnie L. Samuels for critical help, Steve Colluci, and other members of the Cornell EAS faculty for nominating this work for the AMS Father James B. Macelwane Award, and the AMS Fellowship Committee for bestowing the award. Thank you to the anonymous reviewers whose comments improved the overall science of this endeavor. I would like to acknowledge the NOAA Ernest

F. Hollings scholarship program, which provided funding for this research.

REFERENCES

Ackerman, A., O. Toom, J. Taylor, D. Johnson, P. Hobbs, and R. J. Ferek, 2000: Effects of aerosols on cloud albedo: Evaluation of Twomey's parameterization of cloud susceptibility using measurements of ship tracks. *J. Atmos. Sci.,* **57,** 2684–2695.

——, M. Kirkpatrick, D. Stevens, and O. Toown, 2004: The impact of humidity above stratiform clouds on indirect aerosol climate forcing. *Nature,* **432,** 1014–1017.

Adcroft, A., R. Hallberg, and M. Harrison, 2008: A finite volume discretization of the pressure gradient force using analytic integration. *Ocean Modell.,* **22** (3–4), 106–113.

Adler, R., and Coauthors, 2003: The version-2 global precipitation climatology project GPCP monthly precipitation analysis (1979–present). *J. Hydrometeor.,* **4,** 1148–1167.

Albrecht, B. A., 1989: Aerosols, cloud microphysics, and fractional cloudiness. *Science,* **245,** 1227–1230.

AMS, cited 2009: Geoengineering the climate system: A policy statement of the American Meteorological Society. [Available online at http://www.ametsoc.org/policy/2009geoengineeringclimate_amsstatement.pdf.]

Anderson, J., and Coauthors, 2004: The new GFDL global atmosphere and land model AM2–LM2: Evaluation with prescribed SST simulations. *J. Climate,* **17,** 4641–4673.

Anderson, W., A. Gnanadesikan, R. Hallberg, J. Dunne, and B. Samuels, 2007: Impact of ocean color on the maintenance of the Pacific Cold Tongue. *Geophys. Res. Lett.,* **34,** L11609, doi:10.1029/2007GL030100.

——, ——, and A. Wittenberg, 2009: Regional impacts of ocean color on tropical pacific variability. *Ocean Sci.,* **5,** 313–327.

Bickel, J., and L. Lane, 2009: An analysis of climate engineering as a response to climate change. Copenhagen Consensus Center, Copenhagen Consensus on Climate Publ., 57 pp.

Bower, K., T. Choularton, J. Latham, J. Sahraei, and S. Salter, 2006: Computational assessment of a proposed technique for global warming mitigation via albedo-enhancement of marine stratocumulus clouds. *Atmos. Res.,* **82,** 328–336.

Boyd, P. W., 2008: Ranking geo-engineering schemes. *Nat. Geosci.,* **1,** 722–724.

Camargo, S., K. Emanuel, and A. Sobel, 2007a: Use of a genesis potential index to diagnose ENSO effects on tropical cyclone genesis. *J. Climate,* **20,** 4819–4833.

——, A. Sobel, A. Barnston, and K. Emanuel, 2007b: Tropical cyclone genesis potential index in climate models. *Tellus,* **59A,** 428–443.

Collins, W. D., P. J. Rasch, B. A. Boville, J. J. Hack, J. R. McCaa, D. L. Williamson, J. T. Kiehl, and B. Briegleb, 2004: Description of the NCAR Community Atmosphere Model (CAM 3.0). National Center for Atmospheric Research Tech. Rep. NCAR TND 464+STR, 214 pp.

Crutzen, P., 2006: Albedo enhancement by stratospheric sulfur injections: A contribution to resolve a policy dilemma? *Climatic Change,* **77** (3–4), 211–220.

Dai, A., 2006: Precipitation characteristics in eighteen coupled climate models. *J. Climate,* **19,** 4605–4630.

Delworth, T., and Coauthors, 2006: GFDL'S CM2 global coupled climate models. Part I: Formulation and simulation characteristics. *J. Climate,* **19,** 643–673.

Dunne, J., and Coauthors, 2012: GFDL's ESM2 global coupled climate-carbon Earth System Models. Part I: Physical formulation and baseline simulation characteristics. *J. Climate,* **25,** 6646–6665.

Emanuel, K. A., and D. S. Nolan, 2004: Tropical cyclone activity and global climate. Preprints, *26th Conf. on Hurricanes and Tropical Meteorology,* Miami, FL, Amer. Meteor. Soc., 240–241. [Available online at https://ams.confex.com/ams/26HURR/webprogram/Paper75463.html.]

Frank, W., and E. A. Ritchie, 2001: Effects of vertical wind shear on the intensity and structure of numerically simulated hurricanes. *Mon. Wea. Rev.,* **129,** 2249–2269.

Ghate, V., B. Albrecht, P. Kollias, H. Jonsson, and D. Breed, 2007: Cloud seeding as a technique for studying aerosol-cloud interactions in marine stratocumulus. *Geophys. Res. Lett.,* **34,** L14807, doi:10.1029/2007GL029748.

Gnanadesikan, A., and W. Anderson, 2009: Ocean water clarity and the ocean general circulation in a coupled climate model. *J. Phys. Oceanogr.,* **39,** 314–333.

——, K. Emanuel, G. Vecchi, W. Anderson, and R. Hallberg, 2010: How ocean color steers Pacific tropical cyclones. *Geophys. Res. Lett.,* **37,** L18802, doi:10.1029/2010GL044514.

Goldenberg, S., C. Landsea, A. Mestas-Nunez, and W. Gray, 2001: The recent increase in Atlantic hurricane activity: Causes and implications. *Science,* **293,** 474–479.

Hallberg, R., and A. Adcroft, 2009: Reconciling estimates of the free surface height in lagrangian vertical coordinate ocean models with mode-split time stepping. *Ocean Modell.,* **29,** 15–26.

Harrison, M. J., and R. W. Hallberg, 2008: Pacific subtropical cell response to reduced equatorial dissipation. *J. Phys. Oceanogr.,* **38,** 1894–1912.

Hartmann, D., 1994: *Global Physical Climatology,* International Geophysics Series., Vol. 56, Academic Press, 411 pp.

Houghton, J. T., and Coauthors, 2001: *Climate Change 2001: The Scientific Basis.* Cambridge University Press, 892 pp.

Jones, A., J. Haywood, and O. Boucher, 2009: Climate impacts of geoengineering marine stratocumulus clouds. *J. Geophys. Res.,* **114,** D10106, doi:10.1029/2008JD011450.

Karlsson, J., G. Svensson, and H. Rodhe, 1997: Cloud radiative forcing of subtropical low level clouds in global models. *J. Climate Dyn.,* **30** (7–8), 779–788.

Knutson, T., J. Sirutis, S. Garner, G. Vecchi, and I. Held, 2008: Simulated reduction in Atlantic hurricane frequency under twenty-first-century warming conditions. *Nat. Geosci.,* **1,** 359–364.

Korhonen, H., K. Carslaw, and S. Romakkaniemi, 2010: Enhancement of marine cloud albedo via controlled sea spray injections: A global model study of the influence of emission rates, microphysics and transport. *Atmos. Chem. Phys. Discuss.,* **10,** 735–761.

Kravitz, B., A. Robock, O. Boucher, H. Schmidt, K. E. Taylor, G. Stenchikov, and M. Schulz, 2011: The geoengineering model intercomparison project (geomip). *Atmos. Sci. Lett.,* **12,** 162–167.

Lane, L., Ed., 2006: Workshop report on managing solar radiation. NASA Ames Research Center, Carnegie Institute of Washington Department of Global Ecology Rep. NASA/CP-2007-214558, 31 pp.

Latham, J., 1990: Control of global warming? *Nature,* **347,** 339–340.

——, 2002: Amelioration of global warming by controlled enhancement of the albedo and longevity of low-level maritime clouds. *Atmos. Sci. Lett.,* **3,** 52–58.

——, and Coauthors, 2008: Global temperature stabilization via controlled albedo enhancement of low-level maritime clouds. *Philos. Trans. Roy. Soc.,* **A137,** 3969–3967.

——, and Coauthors, 2012: Marine cloud brightening. *Philos. Trans. Roy. Soc.,* **A370,** 4217–4262.

McBride, J., and R. Zehr, 1981: Observational analysis of tropical cyclone formation. Part 2: Comparison of non-developing versus developing systems. *J. Atmos. Sci.,* **38,** 1132–1151.

Merikanto, J., D. Spracklen, G. Mann, S. Pickering, and K. Carslaw, 2009: Impact of nucleation on global CCN. *Atmos. Chem. Phys. Discuss.,* **9,** 12 999–13 037.

Moorthi, S., and M. J. Suarez, 1992: Relaxed Arakawa–Schubert: A parameterization of moist convection for general circulation models. *Mon. Wea. Rev.,* **120,** 978–1002.

Palmer, C., Ed., 2002: The effects of vertical wind shear as diagnosed by the NCEP/NCAR reanalysis data on northeast Pacific hurricane intensity. Preprints, *25th Conf. on Hurricanes and Tropical Meteorology,* San Diego, CA, Amer. Meteor. Soc., 2B.2. [Available online at https://ams.confex.com/ams/25HURR/webprogram/Paper37947.html.]

Peters, K., J. Quass, and H. Grasl, 2011: A search for large-scale effects of ship emissions on clouds and radiation in satellite data. *J. Geophys. Res.,* **116,** D24205, doi:10.1029/2011JD016531.

Platnick, S., and S. Twomey, 1994: Determining the susceptibility of cloud albedo to changes in droplet concentrations with the advanced very high resolution radiometer. *J. Appl. Meteor.,* **33,** 334–347.

Rasch, P. J., S. Tilmes, R. P. Turco, A. Robock, L. Oman, C.-C. Chen, G. L. Stenchikov, and R. R. Garcia, 2008: An overview of geoengineering of climate using stratospheric sulphate aerosols. *Philos. Trans. Roy. Soc.,* **A366,** 4007–4037.

——, J. Latham, and C. Chen, 2009: Geoengineering by cloud seeding: Influence on sea ice and climate system. *Environ. Res. Lett.,* **4,** 045112, doi:10.1088/1748-9326/4/4/045112.

Robock, A., 2008: Whither geoengineering? *Science,* **320,** 1166–1167.

Roeckner, E., L. Bengtsson, J. Feichter, J. Lelieveld, and H. Rodhe, 1999: Transient climate change simulations with a coupled atmosphere–ocean GCM including tropospheric sulfur cycle. *J. Climate,* **12,** 3004–3032.

Rossow, W. B., and R. A. Schiffer, 1991: ISCCP cloud data products. *Bull. Amer. Meteor. Soc.,* **72,** 2–20.

——, and ——, 1999: Advances in understanding clouds from ISCCP. *Bull. Amer. Meteor. Soc.,* **80,** 2261–2287.

Rotstayn, L., 1997: A physically based scheme for the treatment of stratiform clouds and precipitation in large-scale models. I: Description and evaluation of microphysical processes. *Quart. J. Roy. Meteor. Soc.,* **123,** 1227–1282.

——, B. F. Ryan, and J. Katzfey, 2000: A scheme for calculation of the liquid fraction in mixed-phase clouds in large-scale models. *Mon. Wea. Rev.,* **128,** 1070–1088.

Rozendaal, M., C. Leovy, and S. Klein, 1995: An observational study of diurnal variations of marine stratiform cloud. *J. Climate,* **8,** 1795–1808.

Salter, S., G. Sortino, and J. Latham, 2008: Sea-going hardware for the cloud albedo method of reversing global warming. *Philos. Trans. Roy. Soc.,* **A366,** 3989–4006.

Seinfeld, J. H., and S. Pandis, 1997: *Atmospheric Chemistry and Physics: From Air Pollution to Climate Change.* Wiley-Interscience, 1203 pp.

Shevliakova, E., and Coauthors, 2009: Carbon cycling under 300 years of land use change: Importance of the secondary vegetation sink. *Global Biogeochem. Cycles,* **23,** GB2022, doi:10.1029/2007GB003176.

Small, J., P. Chuang, G. Feingold, and H. Jiang, 2009: Can aerosol decrease cloud lifetime? *Geophys. Res. Lett.,* **36,** L16806, doi:10.1029/2009GL038888.

Stevens, B., and G. Feingold, 2009: Untangling aerosol effects on clouds and precipitation in a buffered system. *Nature,* **461,** 607–613.

Twomey, S., 1974: Pollution and the planetary albedo. *Atmos. Environ.,* **8,** 1251–1256.

——, 1977: The influence of pollution on the shortwave albedo of clouds. *J. Atmos. Sci.,* **34,** 1149–1152.

——, 1991: Aerosols, clouds, and radiation. *Atmos. Environ.,* **25A,** 2435–2442.

Vecchi, G., and B. Soden, 2007: Increased tropical Atlantic wind shear in projections of global warming. *Geophys. Res. Lett.,* **34,** L08702, doi:10.1029/2006GL028905.

——, K. Swanson, and B. Soden, 2008: Whither hurricane activity? *Science,* **322,** 687–689.

Wood, R., 2007: Cancellation of aerosol indirect effects in marine stratocumulus through cloud thinning. *J. Atmos. Sci.,* **64,** 2657–2669.

——, 2012: Stratocumulus clouds. *Mon. Wea. Rev.,* **140,** 2373–2423.

Xie, P., and P. Arkin, 1997: Global precipitation: A 17-year monthly analysis based on gauge observations, satellite estimates, and numerical model outputs. *Bull. Amer. Meteor. Soc.,* **78,** 2539–2558.